Electronic Supplementary Material (ESI) for Energy & Environmental Science.

Supporting Information

Aromatic Organic Molecular Crystal with Enhanced π-π Stacking Interaction for Ultrafast Zn-Ion Storage

Haozhe Zhang,[a] *Yuanbin Fang,*[a] *Fan Yang,*[a] *Xiaoqing Liu,*[a] *and Xihong Lu**[a]

[a] *MOE of the Key Laboratory of Bioinorganic and Synthetic Chemistry, The Key Lab of Low-carbon Chem & Energy Conservation of Guangdong Province, School of Chemistry, Sun Yat-Sen University, Guangzhou 510275, People's Republic of China. E-mail: luxh6@mail.sysu.edu.cn*

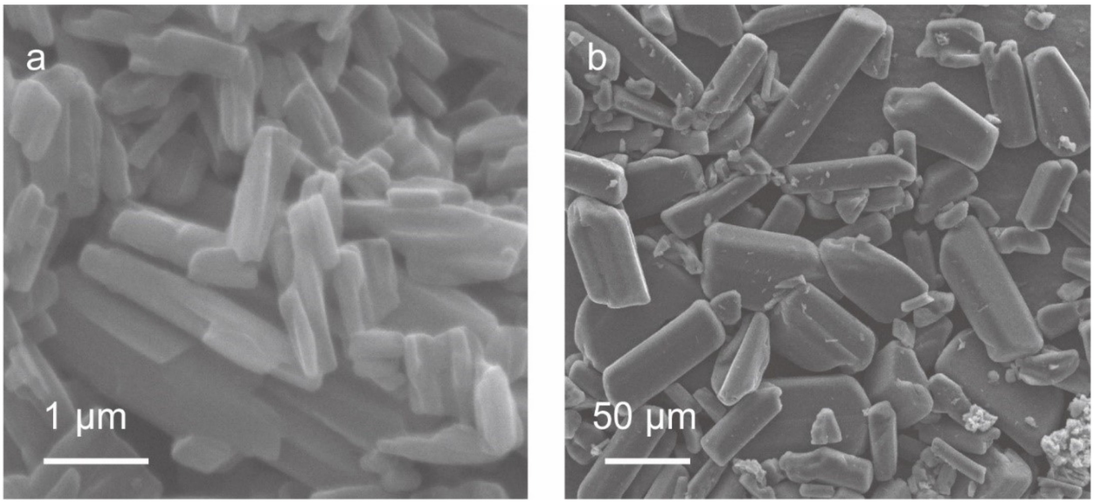

Fig. S1. The SEM images of (a) PMC and (b) π-PMC samples. It can be observed that the PMC are nanorods with a radius range of ~30 to ~200 nm, and the π-PMC are micron rods and micron bulks with a radius range of ~5 to ~25 μm.

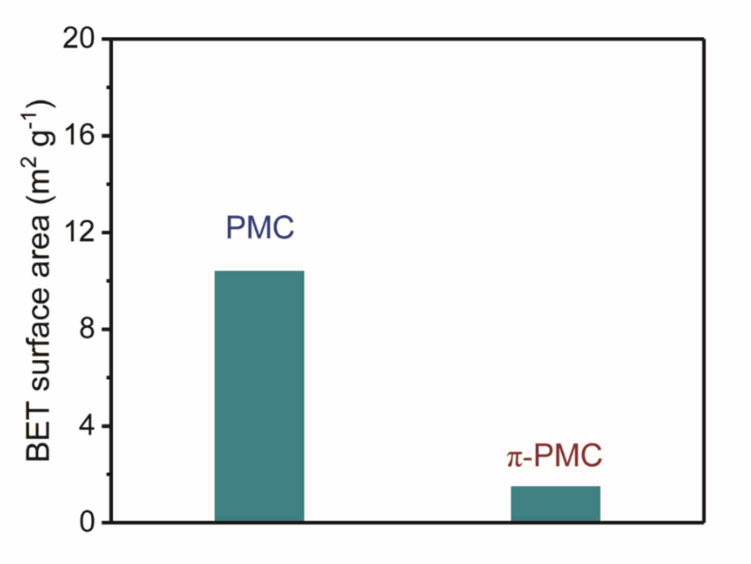

Fig. S2. BET surface area of PMCs. The BET surface area of PMC is 10.4 m^2 g^{-1}, and of π-PMC is 1.5 m^2 g^{-1}.

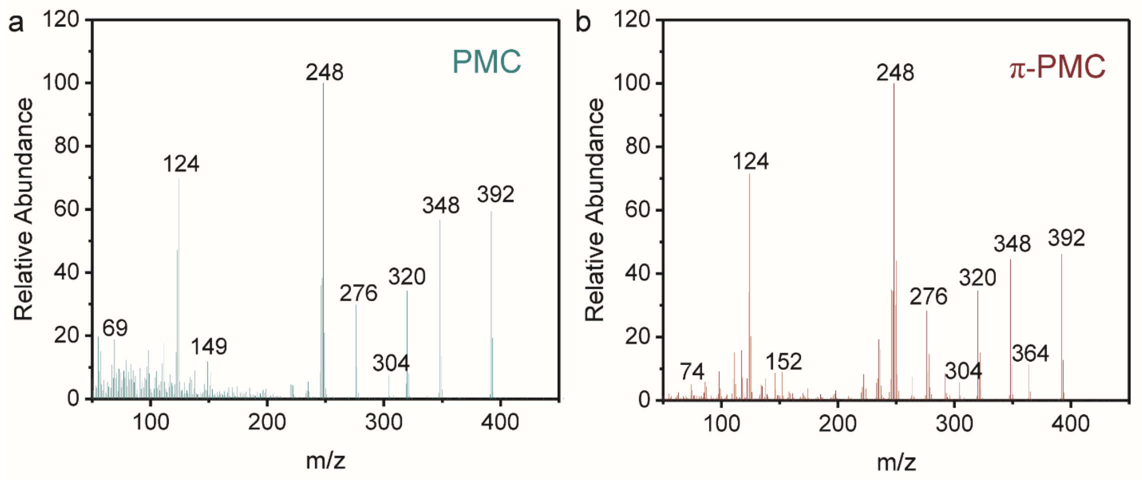

Fig. S3. Electron ionization mass spectrometry results of (a) PMC and (b) π-PMC samples. The main peak at m/z=392 corresponding to the $C_{24}H_8O_6^+$.

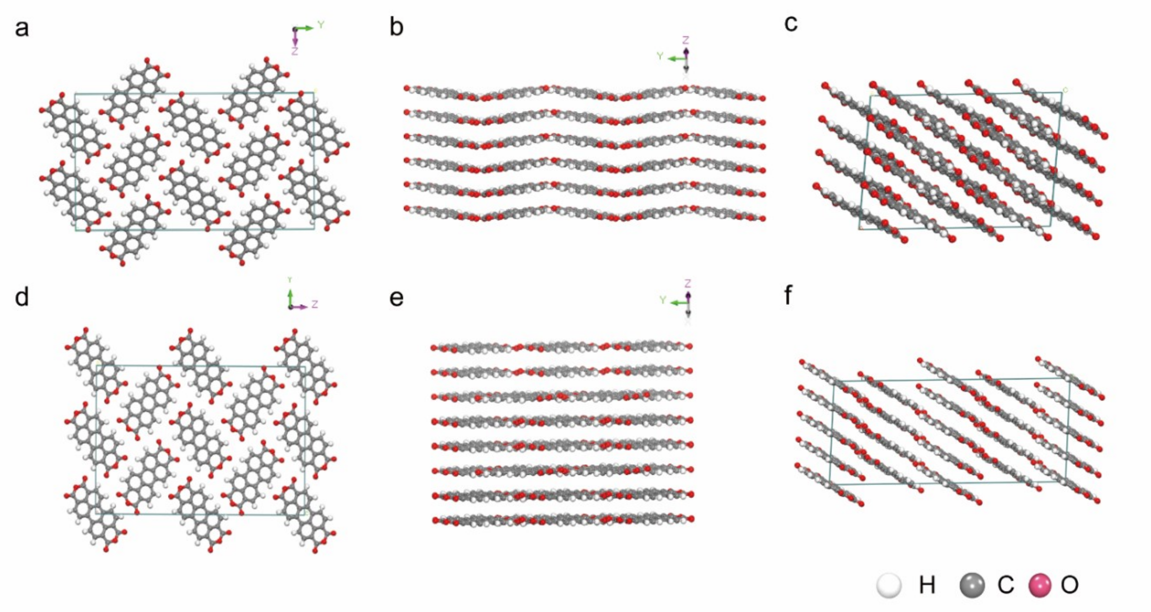

Fig. S4. Schematic illustration of PMC supercells. Different visual angles about the (a-c) PMC and (d-f) π-PMC.

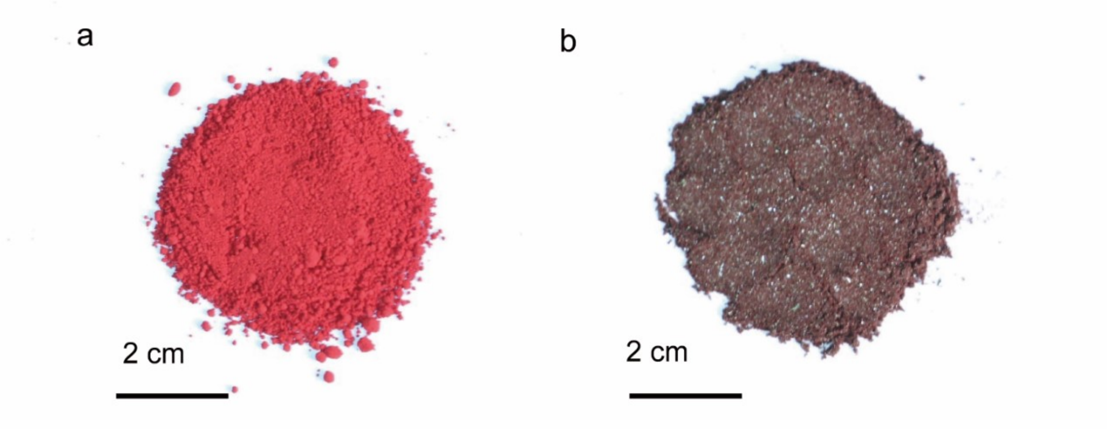

Fig. S5. Optical photograph of (a) PMC and (b) π-PMC samples.

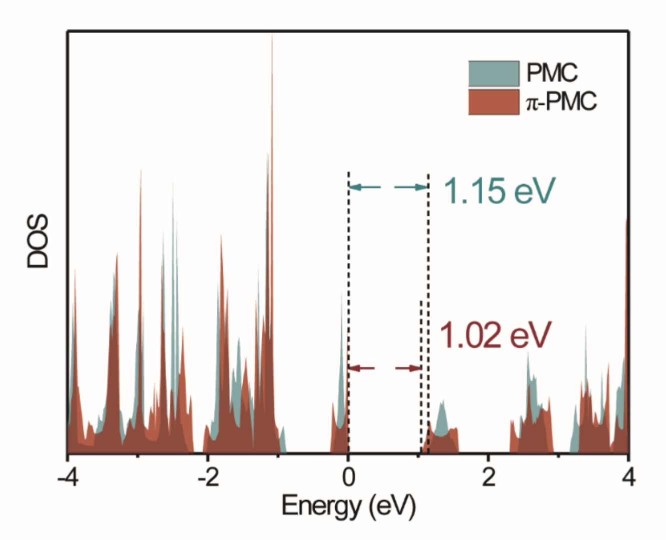

Fig. S6. Calculated density of states (DOS) of PMC bulks. The calculated band gad of PMC is 1.15 eV, and of π-PMC is 1.02 eV.

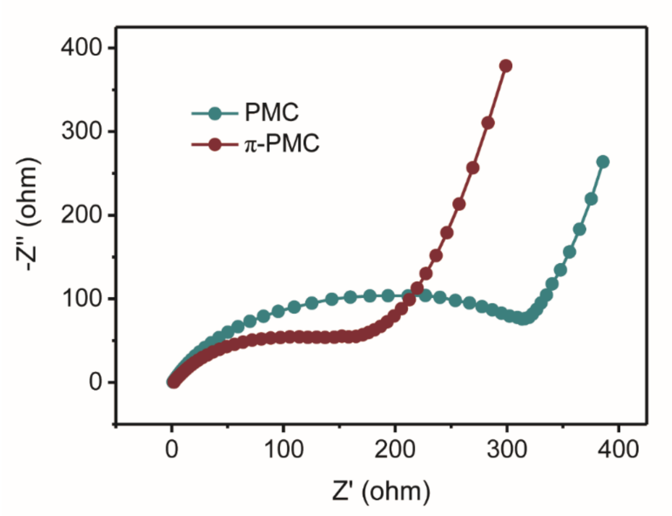

Fig. S7. EIS plots of PMCs. The EIS plots test in a two-electrode cell with the commercial Zn foil as anode and 2 M $ZnCl_2$ as electrolyte.

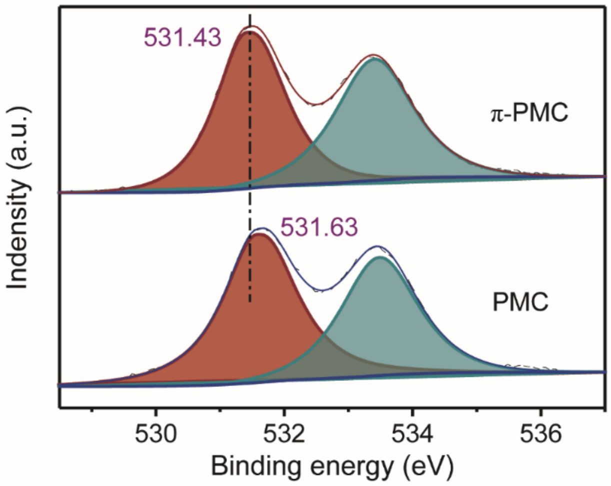

Fig. S8. Core-level O1s XPS spectra of PMCs. Both two samples exhibit two typical O1s peaks, which the red peak corresponding to the C=O and the green peak corresponding to the C-O-C. The C=O peak of PMC is at 531.63 eV, and of π-PMC is at 531.43 eV, which means the O atom become more negatively charged in C=O.

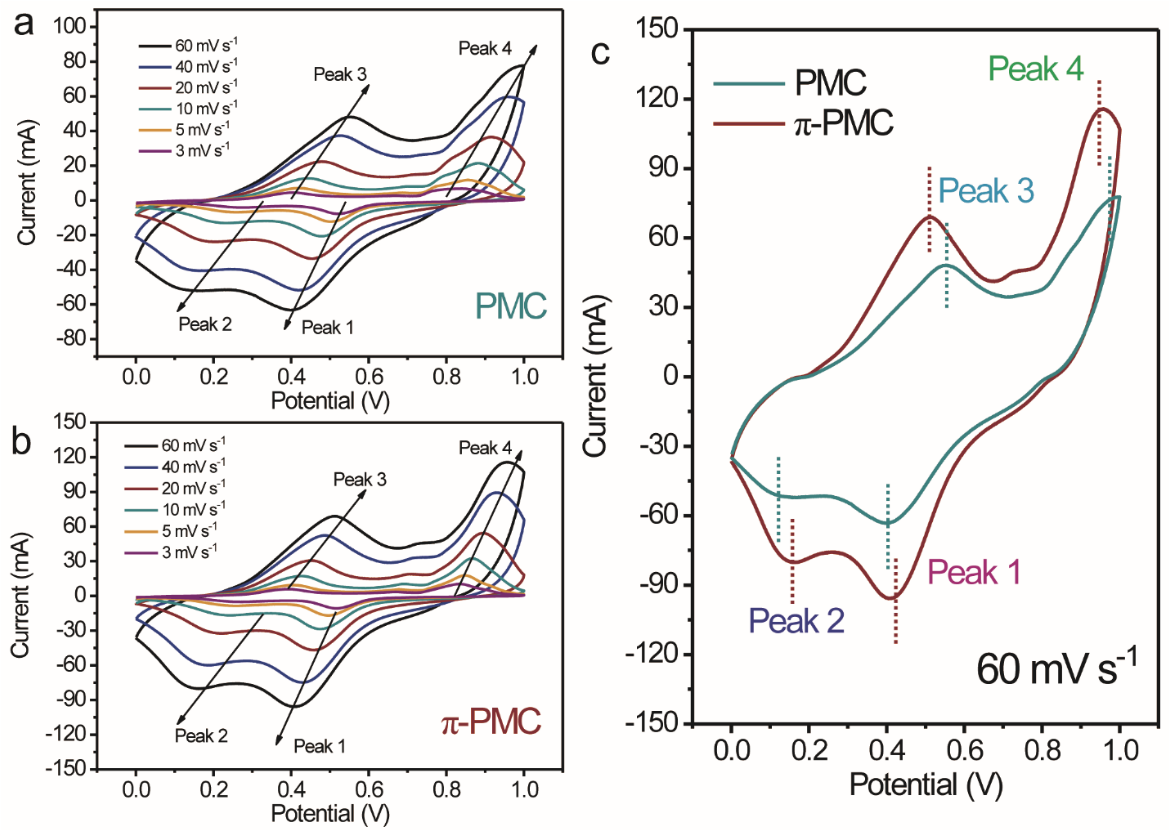

Fig. S9. The CV curves at different scan rates of (a) PMC and (b) π-PMC electrodes. (c) The comparison of PMC and π-PMC electrodes at a scan rate of 60 mV s^{-1}. The π-PMC shows larger area and peak current, as well as a smaller voltage polarization.

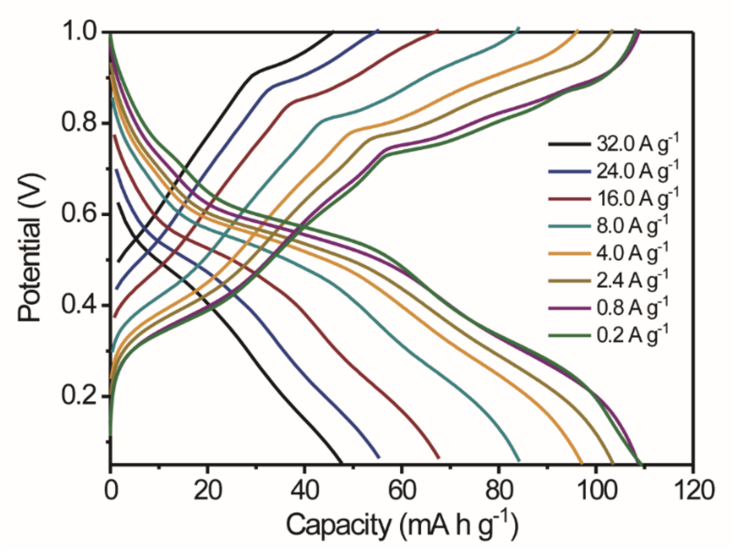

Fig. S10. GCD profiles of PMC electrode from 0.2 A g^{-1} to 32.0 A g^{-1}.

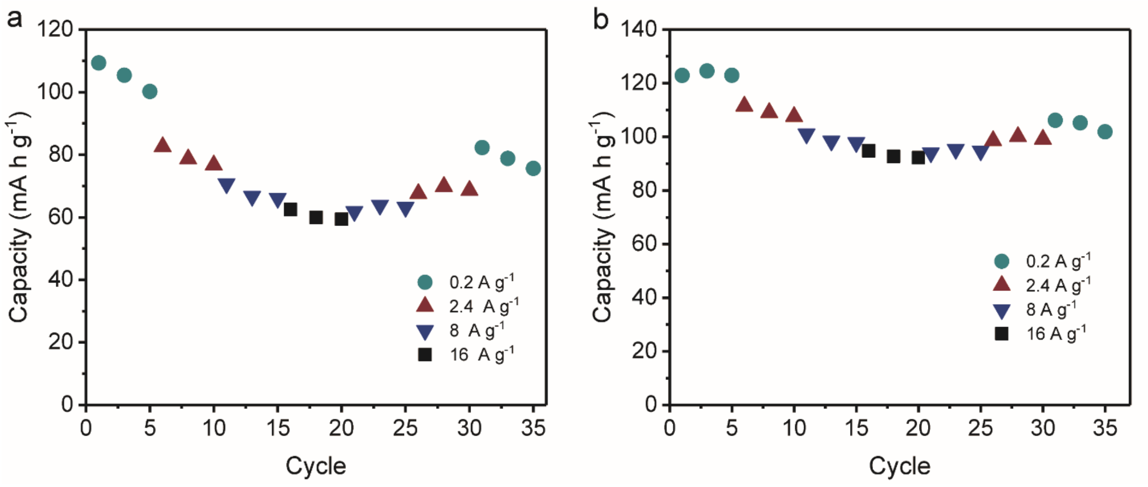

Fig. S11. Rate performances of (a) PMC and (b) π-PMC electrodes at various current densities from 0.2 A g^{-1} to 16 A g^{-1}.

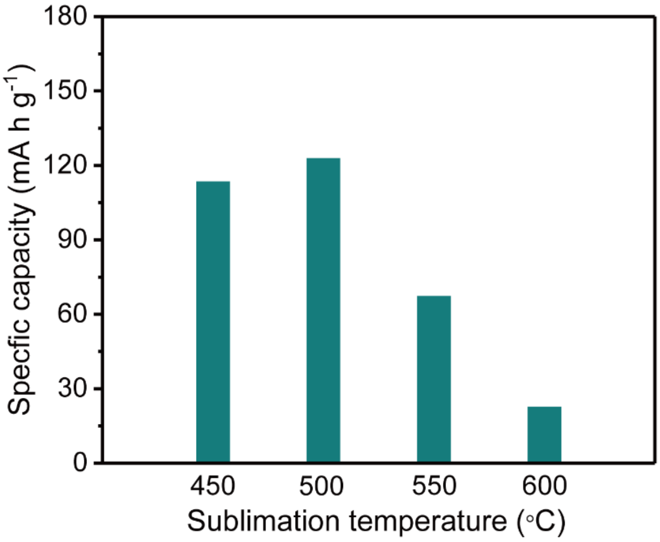

Fig. S12. Specific capacity of PMC cathodes under different sublimation temperature at 0.2 A g^{-1}. Because the sublimation point of the PMC is 450 °C, four temperatures between 450 to 600 °C were chosen for comparison. When the sublimation temperature reached 550 °C or higher, the specific capacity decreases sharply.

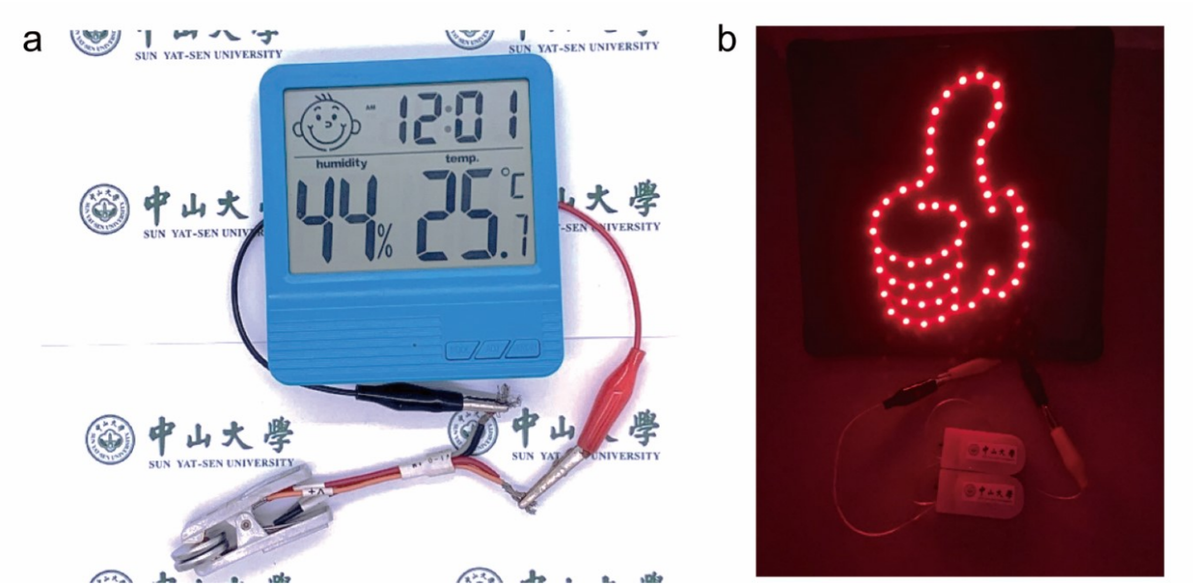

Fig. S13. Demonstrations of Zn//π-PMC cells in daily quick charging use like (a) an electronic timer (>2 h) and (b) a neon light (>20 min) are powered by Zn//π-PMC cells after only about 10 s charging (260.4 C).

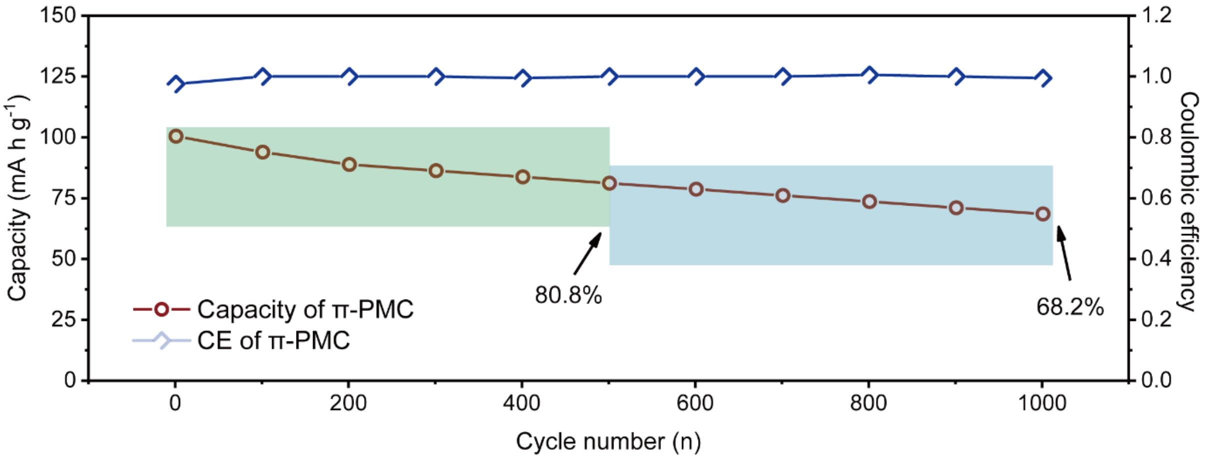

Fig. S14. Cycling stability and coulombic efficiency of the π-PMC cathode at 8 A g^{-1} during the 1000 cycles.

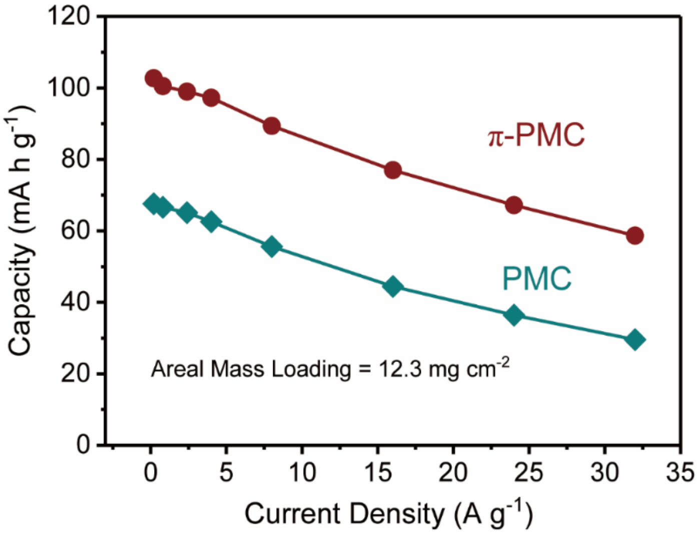

Fig. S15. Specific capacities at different current densities of PMC and π-PMC electrodes at a practical level areal mass loading of 12.3 mg cm^{-2}.

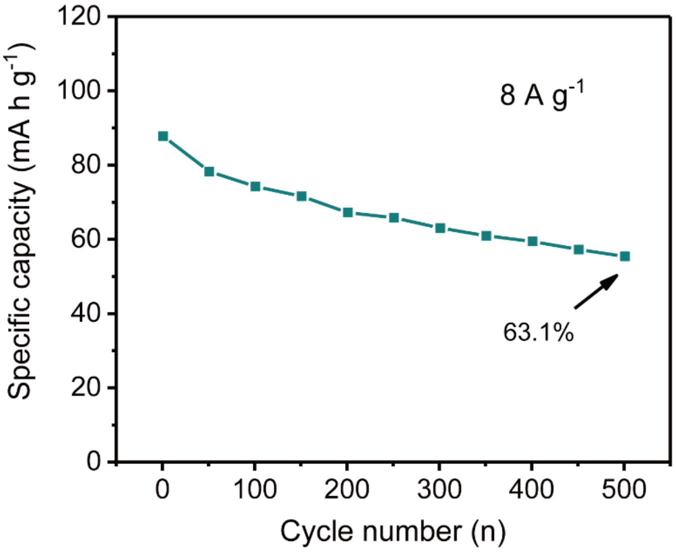

Fig. S16. Cycling stability of π-PMC cathode at a mass loading of 12.3 mg cm^{-2}.

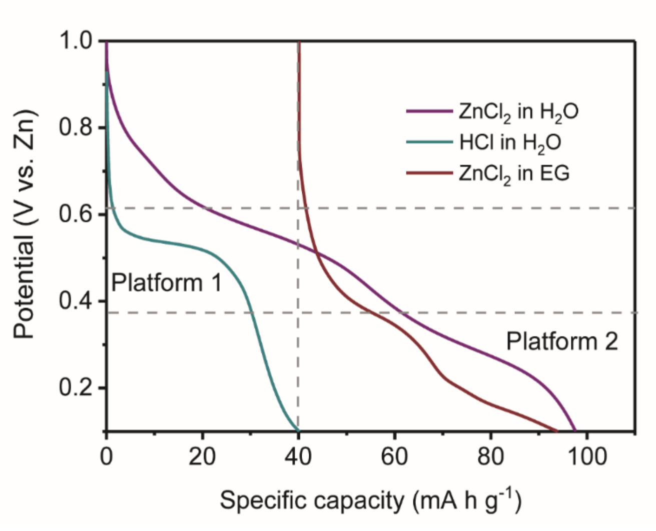

Fig. S17. Discharge curves of π-PMC cathode in different electrolyte at 8 A g^{-1} in a three electrode cell. The three electrode cell use a graphite rod as the counter electrode and a saturated calomel electrode (SCE) as the reference electrode to avoid the influence from Zn electrode.

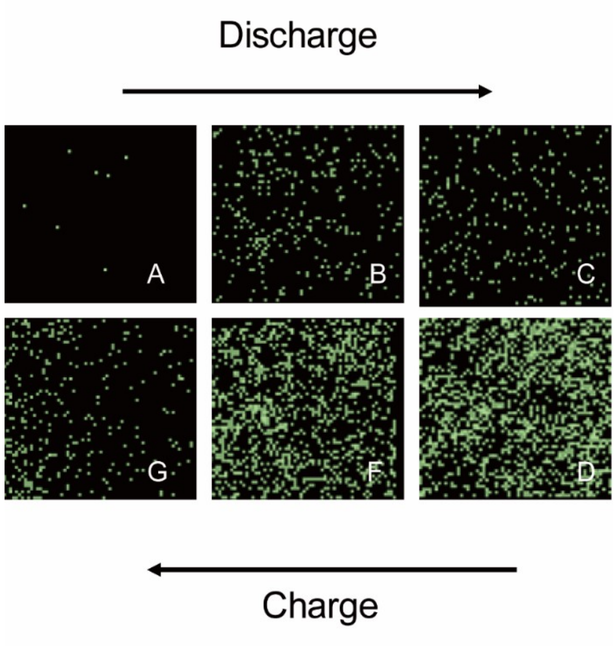

Fig. S18. Ex-situ SEM-EDS mapping of π-PMC. The green spot corresponding to the content of Zn.

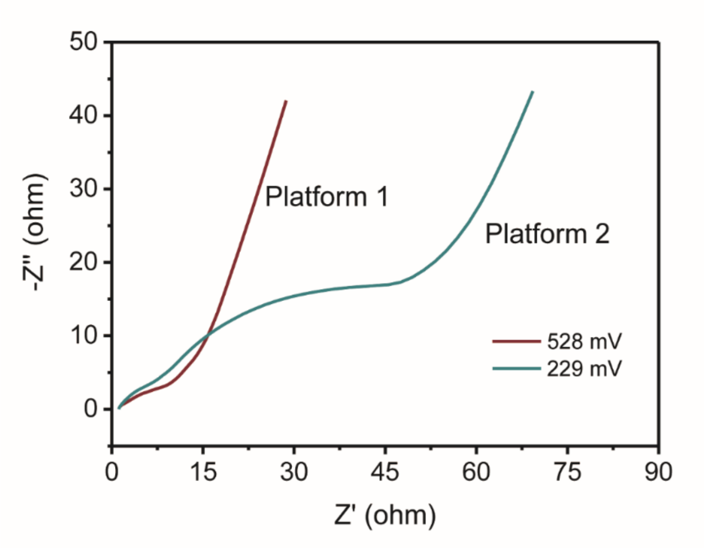

Fig. S19. EIS results of π-PMC electrode at different depth of discharge. The two curves at 528 mV and 229 mV corresponding to the first and the second platform, respectively. The EIS plots are tested in a two-electrode cell as same as the previous tests.

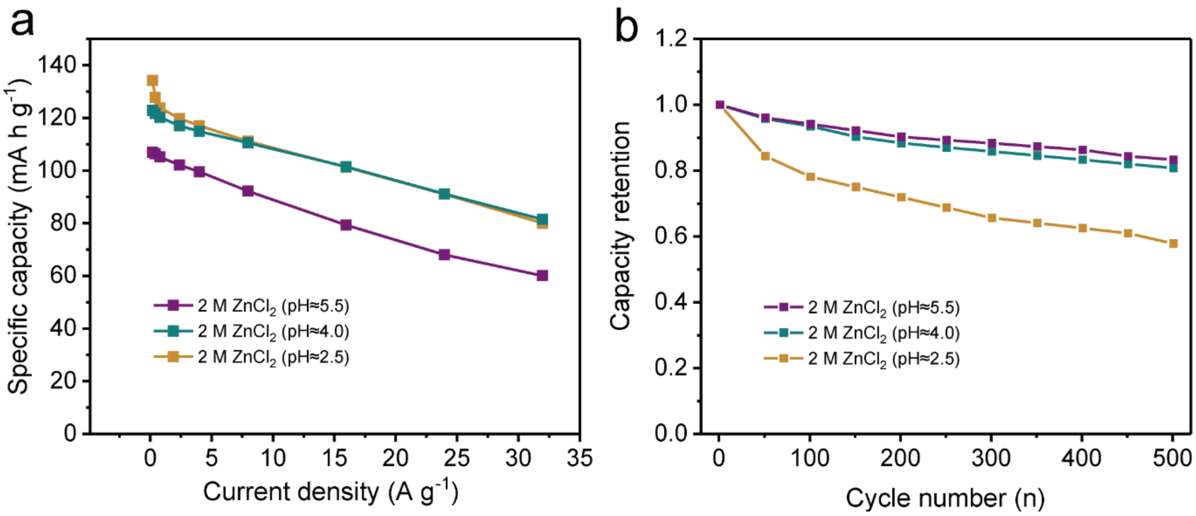

Fig. S20. (a) Specific capacities at different current densities and (b) cycling stabilities at 8 A g^{-1} of π-PMC cathodes in 2 M $ZnCl_2$ electrolytes with different pH values. The specific capacity increases along with the increase of the H^+ concentration, especially at the low current densities. The capacity retention of π-PMC in electrolyte with pH of 2.5 is much worse comparing with other electrolytes. In conclusion, 2 M $ZnCl_2$ electrolyte with pH of 4.0 exhibits the best performance.

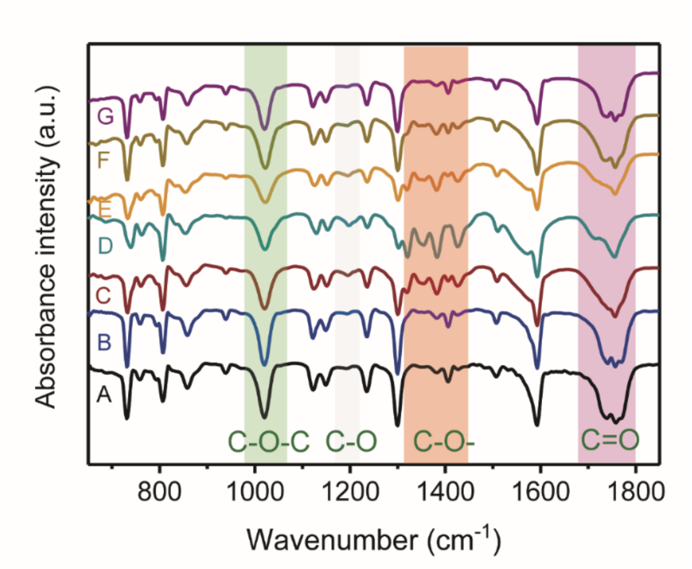

Fig. S21. Ex-situ FT-IR spectra of π-PMC. The peaks at 1375 and 1200 cm^{-1} corresponding to the C-O in enolate groups, and the peaks at 1745 and 1020 cm^{-1} corresponding to the C=O in anhydride groups.

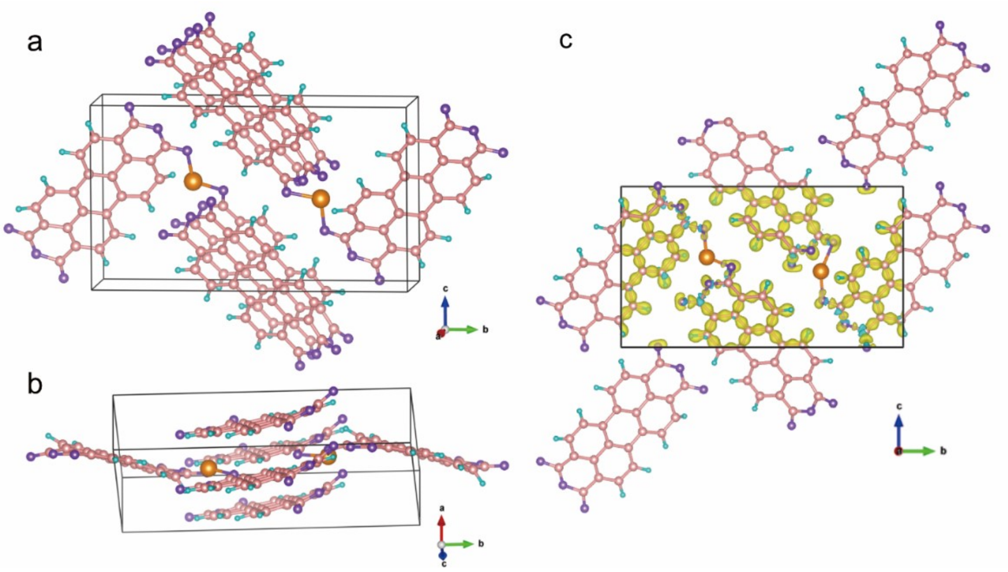

Fig. S22. Simulated Zn inserted PMC structures. (a-b) The structures of PMC after optimization at different visual views. (c) The differential charge density. The Zn ions are position at the 1-D molecular tunnels and interact with the terminal oxygen of carbonyl group, and the structure distorted after the insertion.

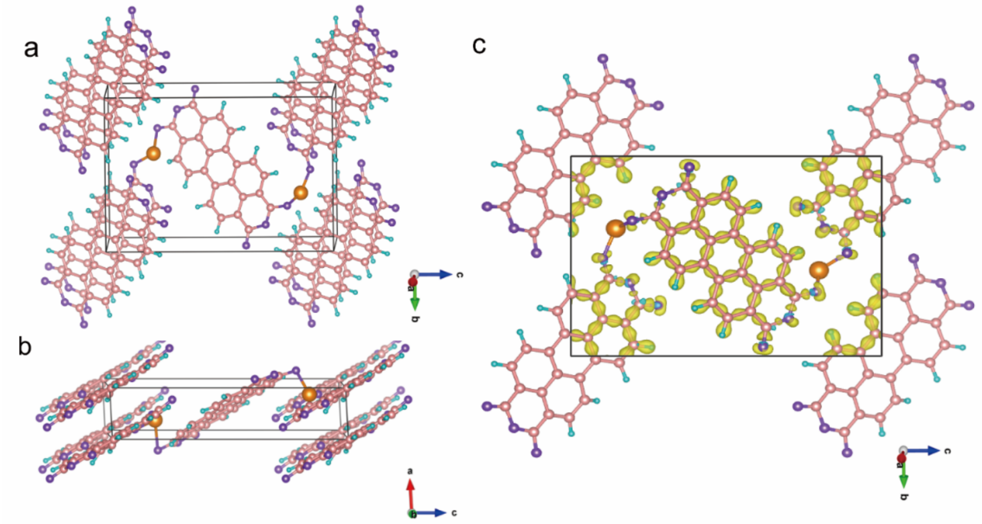

Fig. S23. Simulated Zn inserted π-PMC structures. (a-b) The structures of π-PMC after optimization at different visual views. (c) The differential charge density. The Zn ions are position at the 1-D molecular tunnels and interact with the terminal oxygen of carbonyl group as same as the PMC, but the structure distorted only a little after the insertion.

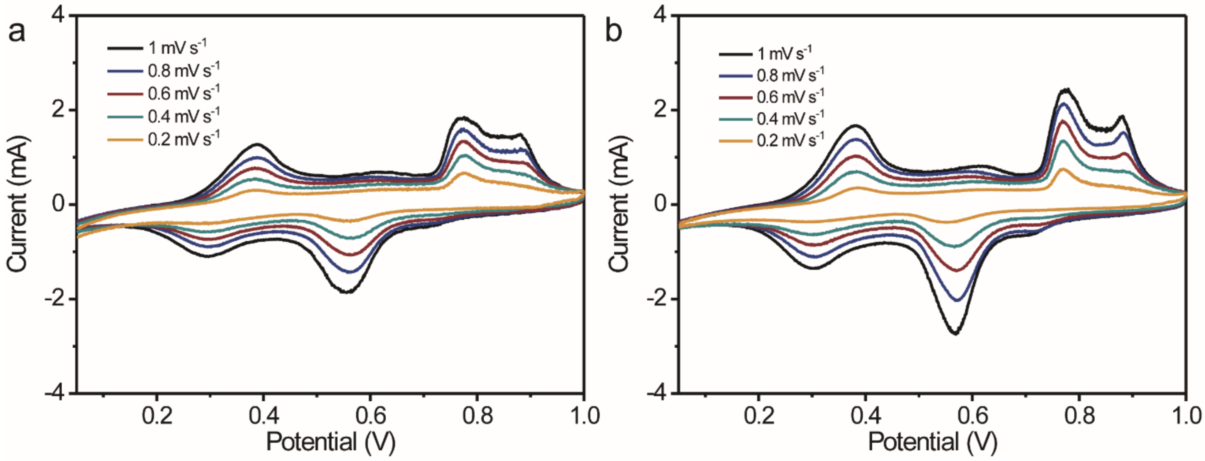

Fig. S24. The CV curves at 0.2–1 mV s^{-1} of (a) PMC and (b) π-PMC electrodes. There has an exponential function relationship between their scan rates (v) and peak currents (i), in which a represents a constant multiplying v and b is the exponent of v. In other words, b value represents the slope linear function of log(i) vs. log(v) curve, which generally has a range of 0.5 to 1. While the b level off to 1, it represents a pseudocapacitance domination at the reaction process, and b level off to 0.5 will represent an ionic diffusion controlled.

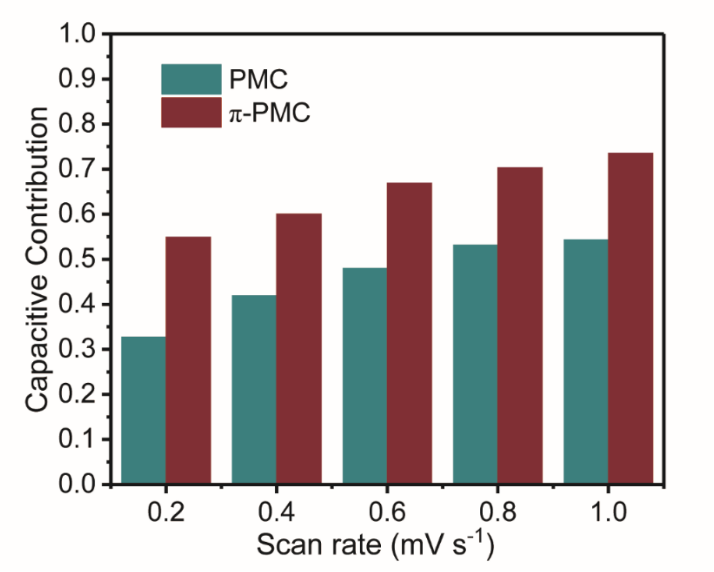

Fig. S25. Corresponding percent of surface capacitive contribution of PMCs. The capacitance contributed by capacitive effects can be calculated based on CV curves at various rates according to the following equation: $i_{(v)} = k_1v + k_2v^{1/2}$. while v stands for scan rate, $i_{(v)}$ stands for current in corresponding scan rate, k_1 and k_2 stand for two constants. In this equation, $k_2v^{1/2}$ stands for the diffusion-controlled current and k_1v stands for the capacitive controlled current.

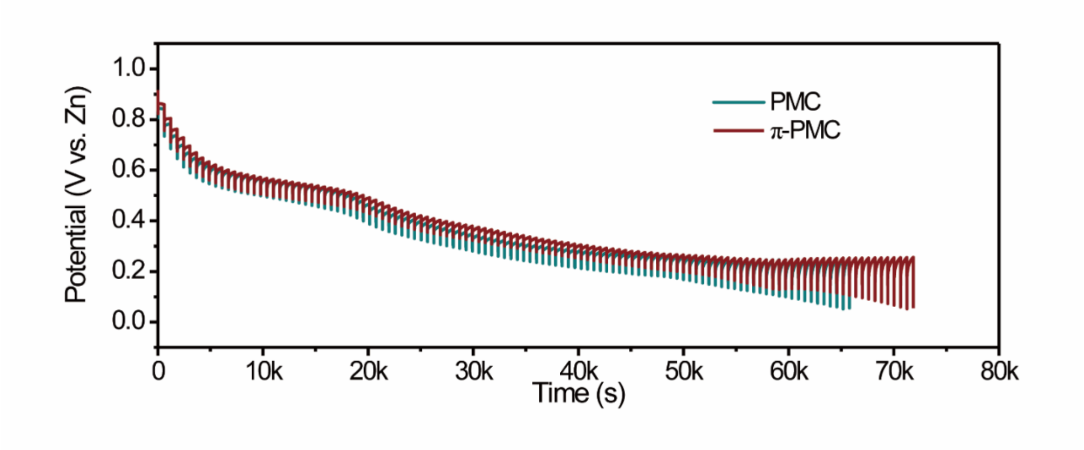

Fig. S26. GITT curves of PMCs. The π-PMC shows a longer discharge time and a smaller overpotential.

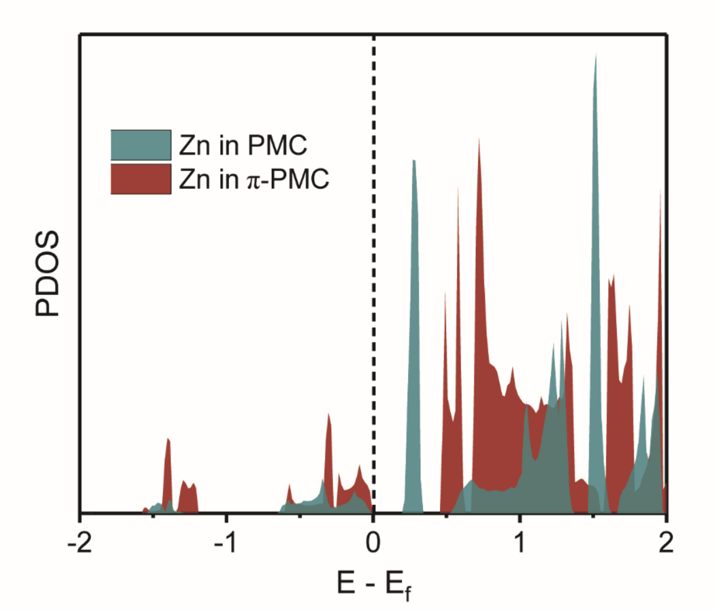

Fig. S27. Change in projected density of states of Zn in two structures. The calculation is based on the structures in Fig. S22 & S23.

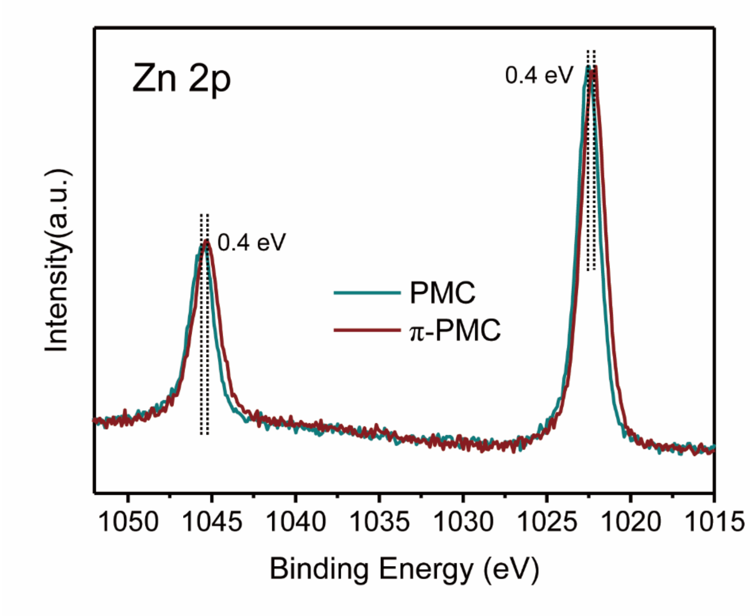

Fig. S28. Zn 2p XPS spectra of PMCs at full-discharging state. The peak of π-PMC has a negative shift of 0.4 eV comparing with one of PMC.

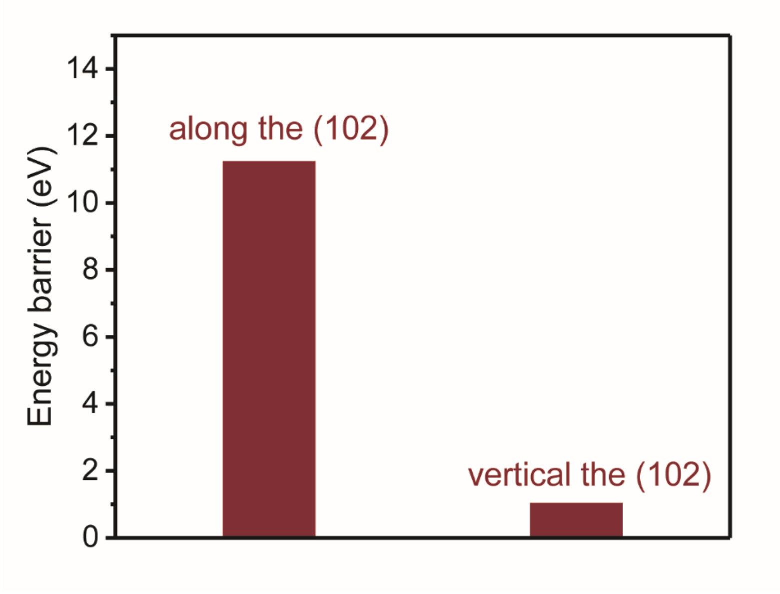

Fig. S29. Diffusion energy barrier of π-PMC along different directions. The two directions are along the (102) plane and vertical the (102) plane.